Fuel 232 (2018) 333–340

Contents lists available at ScienceDirect

Fuel

journal homepage: www.elsevier.com/locate/fuel

Experimental and kinetic modeling investigation on methyl decanoate pyrolysis at low and atmospheric pressures

Yitong Zhai[a], Chengcheng Ao[a], Beibei Feng[a], Qinghui Meng[a], Yan Zhang[a], Bowen Mei[b], Jiuzhong Yang[a], Fuyi Liu[a], Lidong Zhang[a,*]

[a] National Synchrotron Radiation Laboratory, University of Science and Technology of China, Hefei, Anhui 230029, PR China
[b] Key Laboratory for Power Machinery and Engineering of MOE, Shanghai Jiao Tong University, Shanghai 200240, PR China

ARTICLE INFO

Keywords:
Biodiesel
Methyl decanoate
Pyrolysis
Kinetic model
Formation mechanism

ABSTRACT

The pyrolysis of methyl decanoate (MD), an ideal surrogate of biodiesels, was investigated in a flow reactor at the pressures of 30 and 760 Torr and the temperature ranging from 773 to 1198 K. A great variety of pyrolysis products including free radicals, n-alkanes, 1-alkenes, alkynes, unsaturated esters and aromatics were comprehensively observed and identified by employing synchrotron vacuum ultraviolet photoionization mass spectrometry. A new kinetic model for MD pyrolysis was constructed and applied to validate the experimental data. Modeling analyses involving rate of production analysis and sensitivity analysis were performed to help explore the pyrolysis kinetics of MD and the formation mechanisms of key species. The analysis results show that the decomposition of MD is determined by the H-abstraction and unimolecular dissociation reactions during the whole pyrolysis process, whereas the contributions of H-abstraction reactions are enhanced as the pressure elevates. C_4-C_9 unsaturated esters are principally yielded from the β-scission of ester radicals; while the β-scission reactions of MD radicals are responsible for the formation of C_5-C_9 1-alkenes. In addition, 1-alkenes can be further decomposed to form small radicals and molecules. Through the combination reactions such as the reaction routes of $C_3 + C_3$, $C_4 + C_2$ and $C_5 + C_2$, these radicals and molecules can be transformed into benzene and benzyl radical, which are demonstrated as the crucial precursors of polycyclic aromatic hydrocarbons. In conclusion, the pyrolysis of MD would not only significantly enhance the cognitions of various pollutant formation mechanisms but also have a guiding significance for the combustion in the fuel-cooled engine.

1. Introduction

The over-use and over-exploitation of fossil fuels has caused a sequence of environmental problems, such as greenhouse effect, climate change and atmospheric contaminations. Extensive attentions have been raised to the renewable and environmental-friendly biofuels, particularly for biodiesel, which is deemed as the ideal substitutes for conventional diesel fuels [1–3]. As a typical alternative fuel, biodiesels can be used in combustion engines solely or blended with the conventional petroleum-based diesel [4–6]. Due to its unique advantageous properties of high lubricity, cetane number, and flash point, biodiesel fuels can significantly improve the combustion efficiency and reduce the emissions of pollutants such as unburned hydrocarbons, particulate matters and greenhouse gases [7–9].

However, the biodiesel's complicated components of long-carbon-chain fatty acid methyl esters (FAMEs) with 12–20 carbon atoms and the distinct physicochemical properties severely limit the experimental measurements and model simulations [10]. To overcome these difficulties, the viable solution is to seek for representative surrogates with shorter chain lengths to study the combustion chemistry of real biodiesels. Although these typical small esters, such as methyl butanoate and methyl crotonate [11–13], could represent the reactivity of ester moiety satisfactorily for long chain FAMEs, they are not feasible surrogates to study the biodiesel combustion characteristic. Methyl decanoate (MD), on account of its requisite functionality of methyl esters and sufficiently long aliphatic chain, has been regarded as a reasonable surrogate for biodiesels [14].

There has been a continual interest among the research community of MD combustion, covering experiments, mechanisms, and kinetics modeling. As far as the experimental investigations were concerned, much work had been carried out to gain its combustion chemistry under various experimental conditions. For its global combustion parameter measurements, Wang and co-workers [15] determined the laminar burning velocity of MD at atmospheric pressure. Haylett and co-

* Corresponding author.
E-mail address: zld@ustc.edu.cn (L. Zhang).

https://doi.org/10.1016/j.fuel.2018.05.145
Received 3 March 2018; Received in revised form 23 April 2018; Accepted 29 May 2018
Available online 05 June 2018
0016-2361/ © 2018 Elsevier Ltd. All rights reserved.

workers [16] measured the ignition delay times (IDT) of MD using shock tube at 7 atm, temperatures of 1125–1350 K and equivalence ratios of 0.9–0.17. IDTs of MD using shock tube were also carried out by Wang et al. [17] and Li et al. [18]. Wang and co-workers [17] measured the IDTs in reflected shock experiments at temperatures of 653–1336 K, pressures around 15–16 atm, and equivalence ratios of 0.5, 1.0, and 1.5; Li and co-workers [18] obtained the IDTs of MD under high-pressure exhaust gas recirculation.

For flame experiments of MD, Sarathy et al. [19] presented new combustion results in a diffusion flame at 101 and 1013 kPa, temperatures of 900–1800 K and equivalence ratios of 0.25–2.0 using GC/flame ionization detection (FID). A detailed kinetic model was constructed, and served as the basis to develop a skeletal mechanism via direct relation graph. Another flame experiment was carried out by Seshadri and his co-workers [20], they investigated the flame extinction and ignition of MD in laminar non-premixed flames; and calculated the critical conditions of extinction and ignition according to their skeletal mechanism.

In addition, Herbinet et al. [21] reported a detailed kinetic model to describe the low- and high-temperature oxidation of MD on the basis of n-heptane and iso-octane, revealing that the early formation of CO_2 and CO may come from the ester group. Afterwards, they [22] developed a comprehensive kinetic model combing the sub-mechanisms of unsaturated methyl decenoates, which has a good performance with their previous experimental data in a jet-stirred reactor (JSR). Glaude and co-workers [23] obtained the JSR oxidation products of MD at 1.06 bar, temperatures form 500 to 1000 K and with a residence time of 1.5 s by using gas chromatography (GC). A model was also further proposed based on the EXGAS routine to simulate the experimental results. On the other side, based on the experimental achievements, the kinetic models for MD combustion were also performed and developed by Diévart et al. [24], Grana et al. [25] and Luo et al. [26].

Pyrolysis experiments, providing a relatively easy and specific reaction condition, could express the high-temperature chemistry of fuel to advance in biodiesel applications in engines [27]. In other words, not only can it be better to investigate the molecular growth mechanism in combustion kinetic models, but also provide specific species validation on pyrolytic reactions [28]. Furthermore, the pyrolysis of oxygenated fuels has a widespread application in energy conversion and utilization, such as the utilization of fossil fuels [29], bio-energy development [30,31], waste disposal [32], and pollutant emission control [33,34].

To our best acknowledge, just two pyrolysis experimental works of MD were performed [35,36]. Herbinet and co-workers [35] investigated the MD pyrolysis at 800 Torr in JSR by using GC for pyrolysis speciation. In their work, they addressed the formation of carbon oxides, acetaldehyde, as well as the role of retro-ene reactions in MD pyrolysis. Furthermore, Pyl and co-workers [36] measured pyrolysis species of MD in a tubular reactor using a GC/GC-FID/time-of-flight mass spectrometer (TOF-MS) at 1.7 bar and in the temperature range of 873–1123 K. They mostly focused on the formation mechanisms of light alkanes and olefins, formaldehyde, and water. However, a few of large 1-olefins, unsaturated esters and aromatics were also observed in their pyrolysis experiments. So far, the formation mechanisms of these pyrolysis species, especially for aromatics, are still ambiguous under MD pyrolytic condition because of the lack of further experimental and model investigations. Furthermore, their experiments were only confined to the high pressure experimental conditions, which lose sight of the important role of pressure in MD pyrolysis.

In this work, the flow reactor pyrolysis of MD was investigated at 30 and 760 Torr covering temperatures of 773–1198 K by using the synchrotron vacuum ultraviolet photoionization mass spectrometry (SVUV-PIMS). A variety of pyrolysates, in particular, large 1-olefins, unsaturated esters, and aromatics were detected and identified. Their mole fraction profiles versus temperature were also evaluated. A new kinetic model of MD pyrolysis was constructed and used to validate against the new experimental data. Key reactions in MD decomposition and the formation mechanisms of large 1-olefins, unsaturated esters and aromatics were discussed and elucidated with the help of modeling analysis.

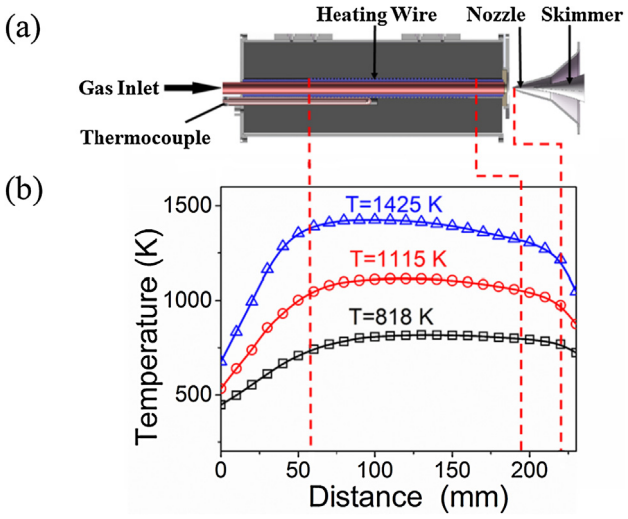

Fig. 1. (a) Schematic diagram of the flow reactor pyrolysis apparatus. (b) Measured temperature profiles along the centerline of the flow tube.

2. Experimental method

The pyrolysis experiments were carried out at the undulator VUV beamline (BL03U), which is connected to the newly upgraded Hefei Light Source (HLS II) of National Synchrotron Radiation Laboratory. Detailed description of BL03U beamline used in this work can be found elsewhere [23]. The pyrolysis equipment schematic diagram is displayed in Fig. 1(a). In summary, the pyrolysis equipment consists of three parts, an electrically heated flow reactor mounted in the pyrolysis chamber, a differentially pumped chamber combing with a molecular beam sampling system, and a photoionization chamber connecting to a home-made reflectron TOF-MS (RTOF-MS) with its mass resolution of ~2000.

In this work, the pyrolysis experiments were performed at 30 and 760 Torr, and the detailed experimental conditions are listed in Table 1. The liquid MD was fed into a vaporizer and after being vaporized it was diluted with Ar at a temperature of 523 K. The total inlet flow rate of MD (1% in volume) and Ar mixture was maintained at 1.0 standard liter per minute. The flow rate of MD was controlled by a liquid chromatography pump, and that of Ar was determined by a mass flow controller. After vaporization, the mixture of MD and Ar was transported to the crystalline α-alumina flow tube with 7 mm inner diameter and 224 mm heated length. The reason why this material was selected is that it could reduce the wall catalytic effects on hydrocarbon and oxygenated fuel pyrolysis [37,38]. The pyrolytic gaseous species were sampled at 5 mm downstream of the tube outlet by a quartz nozzle. When passing through the differentially pumped chamber, the supersonic molecular beam of pyrolysis products was formed. The formed molecular beam entered into the photoionization chamber through a nickel skimmer, where the pyrolysis species were crossed and ionized via the synchrotron VUV light. Eventually, the ions were captured and

Table 1
Experimental conditions of MD pyrolysis.

P (Torr)	*T* (K)	Fuel%	Ar%	Total flow rate (SCCM[a])
30	898–1198 K	1	99	1000
760	773–1048 K	1	99	1000

[a] Standard cubic centimeter per minute.

identified by the RTOF-MS.

The experimental work was employed in two different models. One is to scan the energy of the synchrotron radiation to measure the ionization energy (IE) from the photoionization efficiency curves (PIE) for intermediates identification at a certain pyrolysis temperature. The other one is to scan the temperature to obtain the mole fraction profiles of the pyrolysis species as a function of the temperature at several fixed photon energies (16.32, 14.50, 13.00, 11.00, 10.50, 10.00, 9.50, 9.00 and 8.50 eV). Detailed methods of intermediate measurement and mole fraction evaluation have been introduced elsewhere [39–41]. In general, mole fractions of each species can be calculated at several photon energies as long as the selected energies exceed the IE of the species. Besides, lower photon energies were chosen to calculate the mole fractions of species to avoid possible fragmentation interferences at higher photon energies. The uncertainties of experimental mole fractions are within ± 10% for major products, ± 25% for minor intermediates with known photoionization cross sections (PICSs), and a factor of 2 for those with estimated PICSs. In other words, the uncertainties for mole fractions of major species are within 20%; while for other pyrolysis intermediates, the evaluated uncertainty factors (UFs) range from 1.25 to a factor of 2. To be more detailed, for the mole fraction X of a specific species, the uncertainty range is from the lower limit of X/UF to the upper limit of $X \cdot$ UF, which mainly depends on the accuracy of the used PICS values [42].

Furthermore, temperature profiles along the centerline of the flow tube were measured with the same method in previous studies [43,44], which are depicted in Fig. 1(b). Each temperature profile was named by is maximum temperature (Tmax), which can provide accurate experimental temperature profiles for kinetic modeling. The uncertainties of measured temperatures are around ± 30 K.

3. Kinetic modeling

It is quite well-known that the reactions which play a key role in the pyrolysis process of methyl esters are the H-abstraction reactions to produce ester radicals and relevant small intermediates, and unimolecular dissociation reactions to form various alkyl and other radicals [45]. However, due to the limited pressure-dependent kinetic parameters of unimolecular dissociation for large methyl esters, the common approach to obtain these pressure-dependent rate constants of unimolecular dissociation reactions are obtained by analogy [46]. Therefore in this work, the rate constants of unimolecular dissociation reactions of MD were referred to the analogous reactions of methyl propanoate and its corresponding alkane of n-decane [43,47]. For another unimolecular dissociation type of MD, i.e. methanol elimination reaction, its rate constant was also acquired from the similar reaction of methyl propanoate [47]. For H-abstraction attacked by H, O, OH, CH_3 and C_2H_5, isomerization and β-scission reactions of MD radicals ($C_{11}H_{21}O_2$), their rate constants were either originated from previous MD models [19,35] or adopted by analogy to these similar reactions of n-decane and its radicals [43]. The C_5-C_{10} sub-mechanisms of unsaturated methyl esters, n-alkanes, alkenes, dialkenes and alkyl radicals were derived from n-decane and other methyl esters models [10,35,43,48]. And the C_0-C_4 sub-mechanisms were directly taken from the previous literature models [43,49,50]. Furthermore, some important reactions which are used to better expound the reaction pathways of benzene, benzyl, toluene, styrene, ethylbenzene and indene, such as the recombination of C_3H_3 and H-elimination reaction of ethylbenzene, etc., were adopted from recently reported toluene model [51]. The details of essential reactions, such as unimolecular dissociation and H-abstraction reactions of MD, are listed in Table S1 in the Supplementary Material.

Thermodynamic data of all species were merged in the present model which were directly taken from the abovementioned models [10,35,43,48–51]. The simulation was performed with the measured temperature profiles as input parameters using Plug Flow Reactor (PFR) module in the CHEMKIN-PRO software [52]. A new kinetic model for MD pyrolysis consisting of 286 species and 2165 reactions was constructed in this work.

4. Results and discussion

Lots of pyrolysis species including free radicals such as methyl (CH_3), propargyl (C_3H_3), and allyl (aC_3H_5) radicals, alkynes such as acetylene (C_2H_2) and propyne (pC_3H_4), n-alkanes such as methane (CH_4), ethane (C_2H_6) and propane (C_3H_8), C_2-C_{10} 1-alkenes such as ethylene (C_2H_4), 1-pentene (1-C_5H_{10}) and 1-octene (1-C_8H_{16}), unsaturated esters such as methyl 2-propenoate ($C_4H_6O_2$, MP2D), methyl 4-pentenoate ($C_6H_{10}O_2$, MF4D) and methyl 6-heptenoate ($C_8H_{14}O_2$, MS6D), aromatics like benzene (A1), toluene (A1CH_3) and indene (C_9H_8) were detected and identified during the MD pyrolysis process. Their mole fraction profiles versus the temperature were also evaluated. Modeling analyses consisting of rate of production (ROP) analysis and sensitivity analysis with a 70% fuel conversion were performed at 1173 K, 30 Torr and 973 K, 760 Torr to explore the kinetic chemistry in the decomposition of MD and the formation of crucial species. The sensitivity analysis is related to that how the solution depends on the various parameters contained in a model. To be more explicit, in the software of CHEMKIN-PRO, the local first-order sensitivity coefficients of the mole fractions of the concerned species were considered in a plug flow reactor [41]. And the sensitivity coefficients can be easily obtained from the widely used Jacobian matrix of combustion models [53–55]. Table S2 of the Supplementary Material presents the species involved in discussion below, along with their formulas, nomenclatures and structures.

4.1. Decomposition of methyl decanoate

Fig. 2(a) depicts the experimental and simulated mole fraction profiles of MD. The initial decomposition temperatures of MD at 30 and 760 Torr is 998 K and 873 K, respectively. It is apparent that the initial decomposition temperature decreases dramatically as the pressure increases, which is attributed to the effect of pressure on MD decomposition behaviors. The ROP analysis demonstrates that the consumption of MD is closely related to the unimolecular dissociation and H-

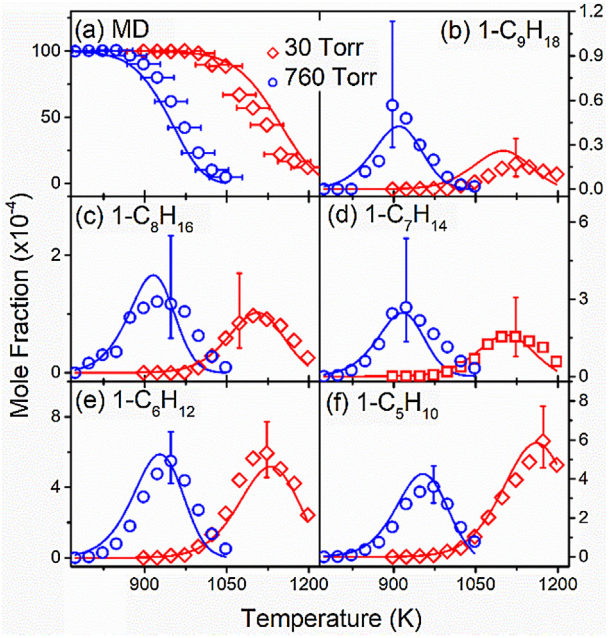

Fig. 2. Experimental (symbols) and simulated (lines) results of MD and C_5-C_9 1-alkenes in MD pyrolysis at 30 and 760 Torr.

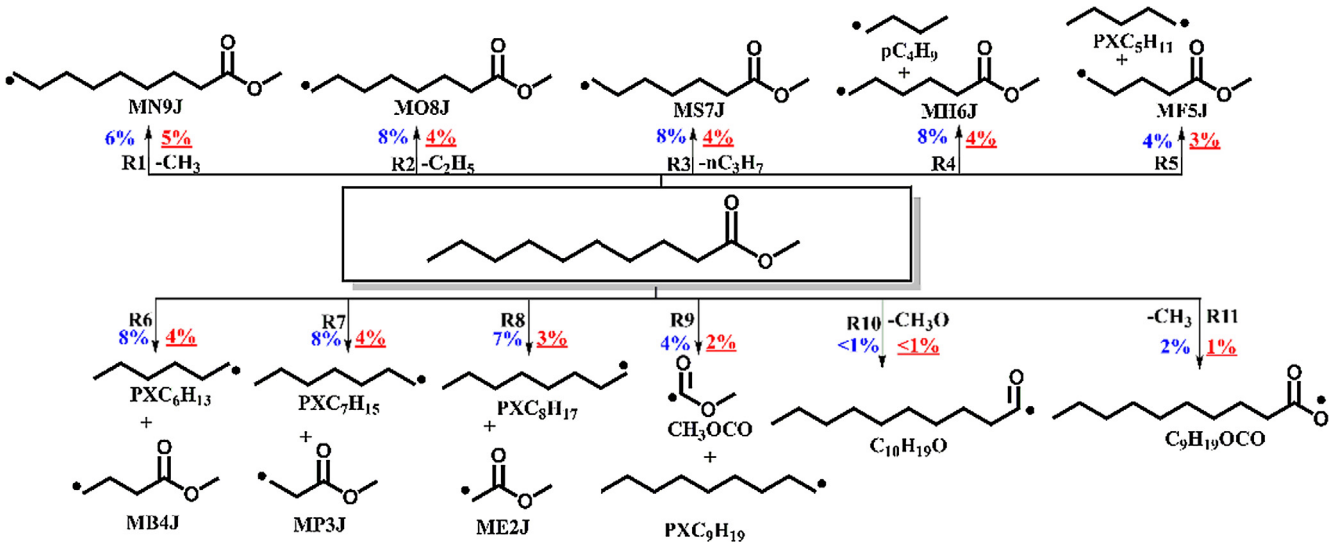

Fig. 3. Reaction network of unimolecular dissociation in MD decomposition at 1173 K, 30 Torr (blue) and 973 K, 760 Torr (red, italicized and underlines). The numbers beside each arrow denotes the percent contribution of specific reaction pathway to the total consumption of MD. (For interpretation of the references to colour in this figure legend, the reader is referred to the web version of this article.)

abstraction reactions. Note that the methanol elimination reaction has almost no contribution to MD consumption.

The reaction network of MD decomposition in Fig. 3 and Fig. 4 indicates that the C–C bond dissociation reactions producing alkyl and methyl ester radicals (R1-R9) are the dominated consumption pathways of MD at low pressure; whereas R10 ($C_{11}H_{22}O_2 = CH_3O + C_{10}H_{19}O$) contributes only negligibly to the consumption since the largest bond dissociation energies (BDEs) of C-O bond in the MD molecule [56]. Overall, the bond dissociation reactions have an approximately 63% and 34% contribution to the consumption of MD at 30 and 760 Torr, respectively. Furthermore, the H-abstraction reactions from the fuel via H and CH_3 radicals also play a vital role in MD consumption, which mainly give rise to ten isomerized MD radicals ($C_{11}H_{21}O_2$). As the elevation of the pressure, the effect of H-abstraction on MD consumption becomes more influential. Around 65% of MD can be decomposed through the H-abstraction reactions (R12-R24) at 760 Torr, while their contributions to MD consumption drop to 37% at 30 Torr. Similar phenomenon was also observed in our previous work on methyl butanoate and methyl crotonate pyrolysis [57]. It is of interest to note that these H-abstraction reactions via CH_3 have inappreciable contribution to MD consumption under the investigated conditions, except reactions R22-R24. This is because that the energy barriers of C–H bonds in these reactions are relatively low in comparison with those C–H bonds of other reactions [58]. The ROP analysis also indicates that the reactions producing MD2J (e.g., R12 and R22) have respectively the highest contribution for MD consumption at both pressures, which is due to the lowest energy barriers of C–H bonds at α-site of the ester moiety in MD molecule [56]. Furthermore, these two H-abstraction reactions via H atom (R20 and R21) have lower contributions to MD decomposition at both pressures. The chief reason is that the dissociation energies of C–H bond at these two sites are relatively high (102.1 kcal mol^{-1} for R20 and 101.1 kcal mol^{-1} for R21 [56]).

Fig. 5 displays the sensitivity analysis of MD at 30 and 760 Torr, respectively. It is obvious that the unimolecular dissociation and H-abstraction reactions are very sensitive to the MD consumption at both pressures, which is in accordance with the ROP analysis. The sensitivity analysis also unambiguously demonstrates that the H-abstraction reactions have larger sensitivity coefficients at atmospheric pressure, and the unimolecular dissociation reactions are more sensitive at low pressure.

4.2. Formation and consumption of C_5-C_9 1-alkenes

A series of 1-alkenes were observed in this work, especially C_5-C_9 1-alkenes. Results of C_5-C_9 1-alkenes from experiments and simulations are presented in Fig. 1b–f. In general, present model can reproduce the

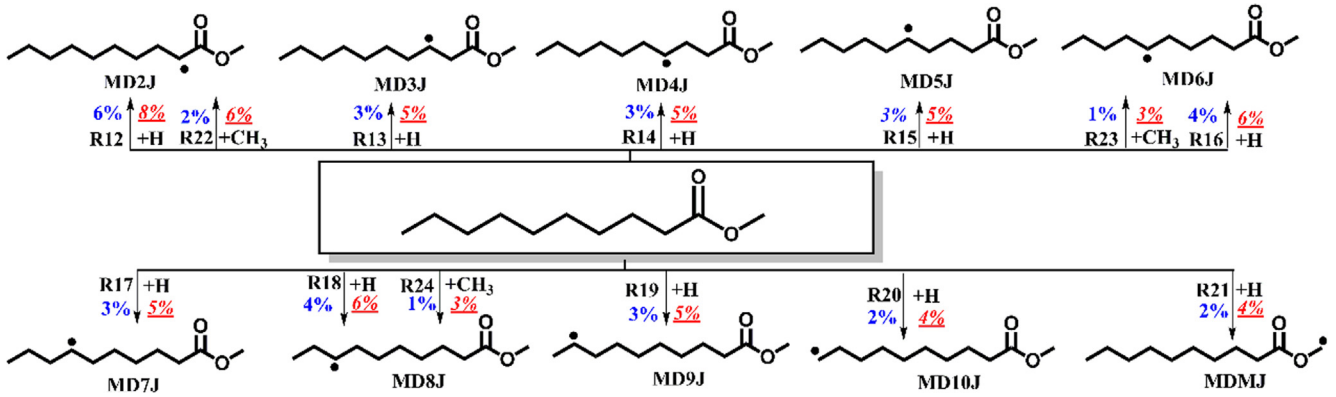

Fig. 4. Reaction network of H-abstraction reactions in MD decomposition at 1173 K, 30 Torr (blue) and 973 K, 760 Torr (red, italicized and underlines). The numbers beside each arrow denotes the percent contribution of specific reaction pathway to the total consumption of MD. (For interpretation of the references to colour in this figure legend, the reader is referred to the web version of this article.)

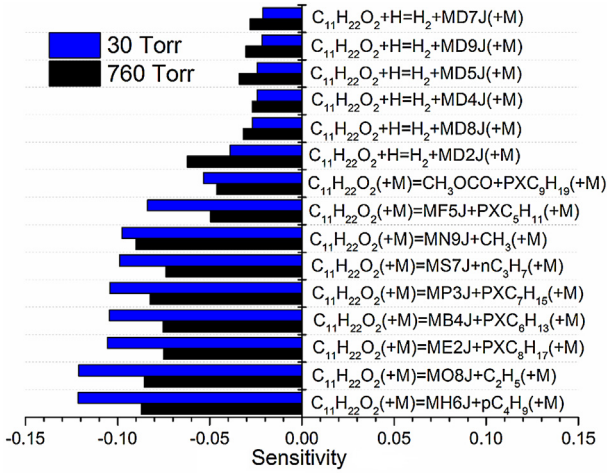

Fig. 5. Sensitivity analysis of MD at 1173 K, 30 Torr and 973 K, 760 Torr.

formation tendency satisfactorily. The ROP analysis from Fig. 6 demonstrates that C_5-C_9 1-alkenes are mostly produced via β-C–C scissions of MD radicals. Among these MD radicals, MD6J radical is the most abundant products which can be further decomposed to form 1-hexene (1-C_6H_{12}). Hence taking 1-C_6H_{12} as an example to investigate the formation routes of large 1-alkenes. Due to the quite similar formation pathways between C_7-C_9 1-alkenes and 1-C_6H_{12}, their formation mechanisms will not be discussed herein.

The majority of 1-C_6H_{12} is produced from the β-C–C scission reaction of MD6J at both pressures; while the β-C–C scission reactions of C_7-C_9 alkyls, containing S2XC$_7$H$_{15}$, S3XC$_8$H$_{17}$ and S4XC$_9$H$_{19}$, only have a bit contribution to 1-C_6H_{12} formation. For the source of MD6J radical, it can be yielded from the H-abstraction of MD and the isomerization of MD2J. As for these three alkyls of S2XC$_7$H$_{15}$, S3XC$_8$H$_{17}$ and S4XC$_9$H$_{19}$, they are primarily derived from the isomerization reactions of PXC$_7$H$_{15}$, PXC$_8$H$_{17}$ and PXC$_9$H$_{19}$. As the pressure elevated, the contributions of β-C–C scissions of C_7-C_9 alkyls gradually decrease. This phenomenon can be interpreted by that the bond dissociation reactions of MD become less competitive at high pressure, which yield only a small amount of

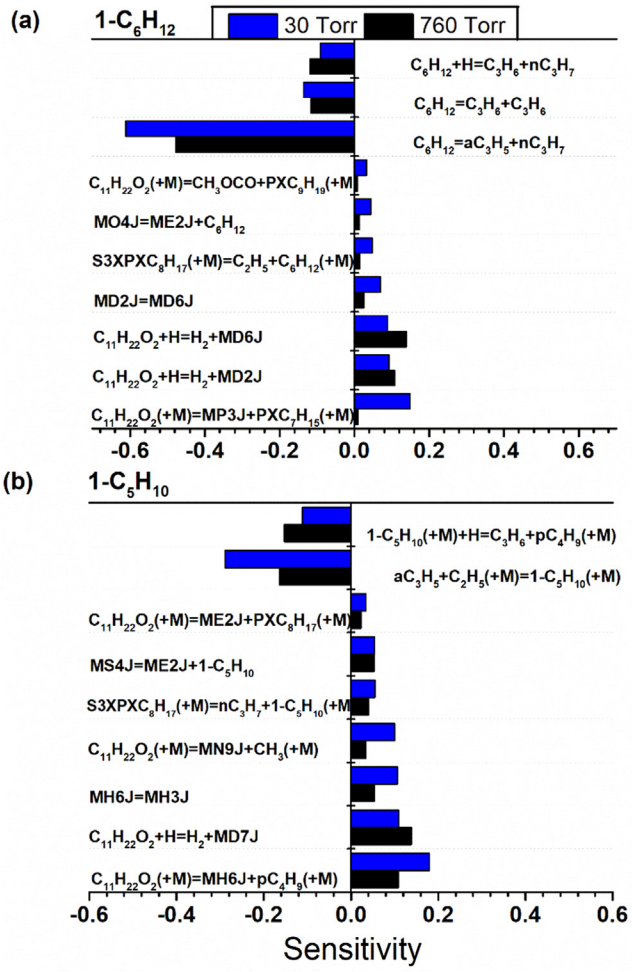

Fig. 7. Sensitivity analysis of (a) 1-C_6H_{12} and (b) 1-C_5H_{10} at 1173 K, 30 torr and 973 K, 760 Torr.

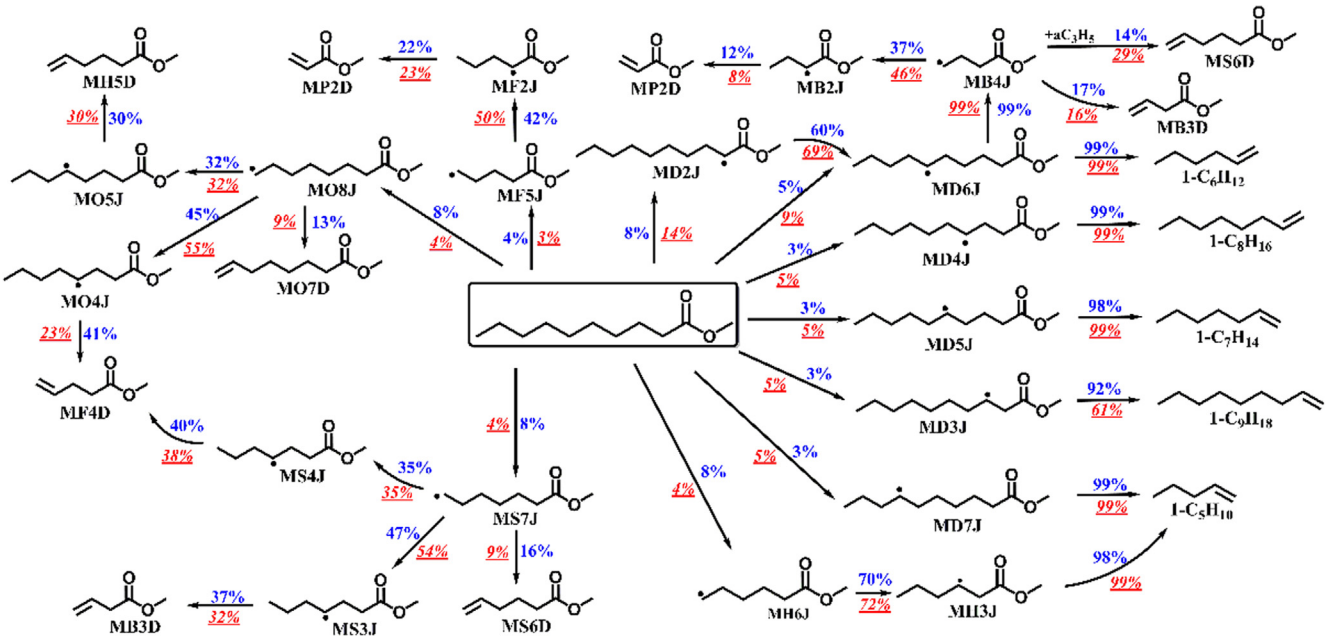

Fig. 6. Formation network of C_5-C_9 1-alkenes and C_4-C_9 unsaturated esters at 1173 K, 30 Torr (blue) and 973 K, 760 Torr (red, italicized and underlines). The numbers beside each arrow denotes the percent contribution of specific reaction pathway to the total consumption of the species on the source side of the arrow. (For interpretation of the references to colour in this figure legend, the reader is referred to the web version of this article.)

PXC_7H_{15}, PXC_8H_{17} and PXC_9H_{19} radicals. As presented the sensitivity analysis of 1-C_6H_{12} in Fig. 7(a), same as the ROP analysis, it also reveals that the H-abstraction reactions to form MD2J and MD6J are very sensitive to the formation of 1-C_6H_{12} at 760 Torr. Moreover, the bond dissociation reaction to produce PXC_7H_{15} has the highest sensitivity to the formation of 1-C_6H_{12} at 30 Torr, coinciding with that the β-C–C scission of $S2XC_7H_{15}$ has a higher contribution to form 1-C_6H_{12} in comparison to $S3XC_8H_{17}$ and $S4XC_9H_{19}$ on the basis of ROP analysis (not shown in Fig. 6). Then this is explained by that the BDEs of relevant C–C bond is quite low [59], which is more facile to be broken to produce PXC_7H_{15} radical.

As for 1-C_5H_{10}, except the β-C–C scission of MD7J, its formation is also controlled by the β-C–C scission of MH3J, which is the product of MH6J via isomerization reaction. The ROP analysis shows that the β-C–C scission of MD7J becomes more important as the pressure increased to 760 Torr because of the elevated contributions of H-abstraction reactions for MD consumption at high pressure. Sensitivity analysis plotted in Fig. 7(b) also proves that the generations of MH6J and MD7J radicals are tremendously sensitive to the formation of 1-C_5H_{10}.

It is concluded that C_5-C_9 1-alkenes can be consumed via analogous reactions, or rather, the bond dissociation reactions, retro-ene reactions and bimolecular reactions. Here 1-C_6H_{12} is also selected as an example. Its consumption is dominated by C(3)-C(4) bond dissociation (1-C_6H_{12} = aC_3H_5 + nC_3H_7) to produce aC_3H_5 and n-propyl radical (nC_3H_7) at both pressures, which is in accordance with the sensitivity analysis. This is caused by that the very weak allylic C(3)-C(4) bond compared with other C–C bonds [60]. Furthermore, the additional reaction routes, i.e. the retro-ene reaction to produce propene (C_3H_6) and the bimolecular reaction to produce C_3H_6 and nC_3H_7, also have a portion contribution to the consumption of 1-C_6H_{12}. This is also fully manifested via the sensitivity analysis.

4.3. Formation and consumption of C_4-C_9 unsaturated esters

Fig. 8 illustrates the experimental and simulated results of C_4-C_9 unsaturated esters. In general, their formations are dominated by the β-scission of methyl ester radicals at both pressures. The reaction network of their formations at both pressures is also exhibited in Fig. 6. To be more detailed, Fig. S1 of the Supplementary Material shows all of the major possible formation channels for C_4-C_9 unsaturated esters. For methyl 7-octenote (MO7D), its formation is totally controlled by the β-C–H scission of MO8J radical because of the lower energy barriers of C–H bond compared with C–C bond. For MS6D, it is mostly yielded via three different channels, which are β-C–H scission of MS7J, β-C–C scission of MD6J and the combination reaction of MB4J and aC_3H_5. Among these formation pathways, the first reaction channel makes the greatest contributions to MS6D at 30 Torr; while at 760 Torr, the last reaction route becomes the most important one. This indicates that the pressure serves a vital role in species formation. Or to be more precise, MS7J can be largely produced at 30 Torr via C–C dissociation reaction; while MB4J can be formed by the reaction sequence of MD/MD2J → MD6J → MB4J. Both MD2J and MD6J can be generated in large amounts by H-abstraction reactions at 760 Torr.

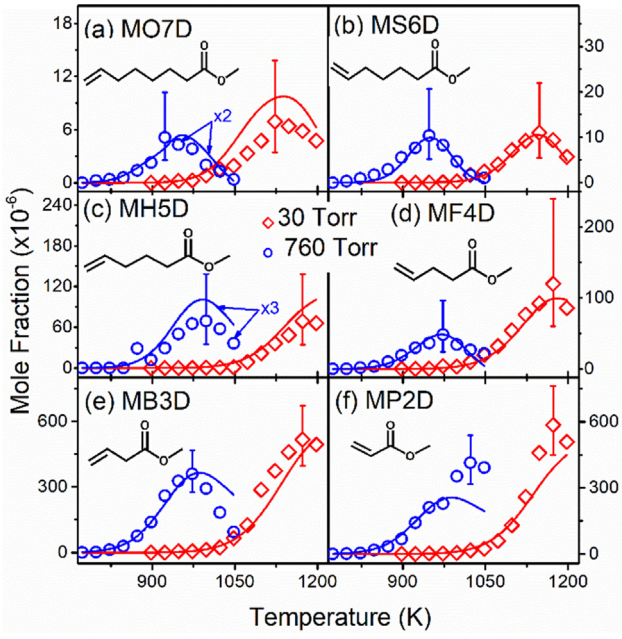

Fig. 8. Experimental and simulated results of C_4-C_9 unsaturated methyl esters in MD pyrolysis at 30 and 760 Torr.

For MF4D and methyl 5-hexenoate (MH5D), their formations are entirely controlled by the β-C–C scission of two different pairs of radicals. Or rather, MO4J and MS4J radicals are responsible for the formation of MF4D; MO5J and MS5J radical are related to the formation of MH5D. Furthermore, the generation pathways for MB3D are either from the decomposition of MS3J radical via β-C–C scission or from the β-C–H scission of MB4J radical. MP2D is mainly originated from four different formation channels, i.e. the β-C–H scission of MP3J and MP2J and the β-C–C scission of MB2J and MF2J, which have an around lumped contribution of 70% at both pressures.

It should be stressed that the maximum mole fraction concentrations of unsaturated esters gradually increases with the decreasing carbon chain length at both pressures. Similar phenomena were also observed from previous pyrolysis and oxidation studies of MD [19,21,35]. This may be that the formation channels of unsaturated esters become more diversified with the decreasing carbon chain length. After their formation, they can be consumed via various routes. For small unsaturated esters, i.e. MP2D and MB3D, their consumptions are mainly determined by H-addition reactions; while for C_6-C_9 unsaturated esters, the H-addition, bond dissociation and bimolecular reactions are the dominated consumption pathways. Besides, the retro-ene reactions producing C_3H_6 and small unsaturated esters also consume these unsaturated esters of MH5D, MS6D and MO7D. As a result, C_4-C_9 unsaturated ester can be produced via β-scission of a sequence of methyl ester radicals; and can also be consumed via various reaction channels, i.e. H-addition, bond dissociation, bimolecular and retro-ene reactions.

4.4. Formation of aromatics

Aromatics consisting of benzene, toluene, styrene ($A1C_2H_3$), ethylbenzene ($A1C_2H_5$) and indene were obtained in this work with quite high mole concentrations. The experimental and simulated results are labelled in Fig. 9. However, possibly due to the very low concentrations, several aromatics were not observed at 30 Torr. Therefore, the formation pathways of aromatics are only discussed based on the kinetic modeling performed at 760 Torr. The reaction network of aromatic formation at 760 Torr was depicted in Fig. 10. As the most important aromatic product in MD pyrolysis, benzene is formed by multiple channels including the isomerization of fulvene and the combination of small radicals and molecules such as C_4H_4 + C_2H_3, pC_3H_4 + C_3H_3, aC_3H_4 + C_3H_3 and C_3H_3 + C_3H_3. For the important precursors of benzene, these two C_3 + C_3 channels (e.g., C_3H_3 + aC_3H_5 and C_3H_3 + C_3H_3) are the key reaction steps for fulvene's production. Considering that the formation of fulvene is from C_3H_3-based and other reactions, C_3 + C_3 channels decide the formation of most benzene. Note that these small radicals and molecules are principally produced through the decomposition of 1-alkenes (see Fig. 10).

In addition, the simulation reveals that benzyl radical ($A1CH_2$), which is primary produced via the combination of C_5H_5 and C_2H_2, plays a significant role in the formation of other aromatics. Toluene is largely

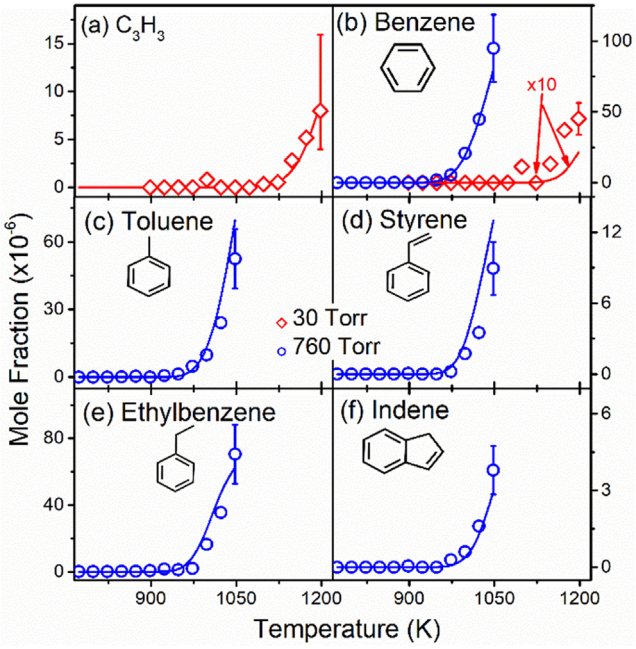

Fig. 9. Experimental and simulated results of propargyl radical and aromatics in MD pyrolysis at 30 and 760 Torr.

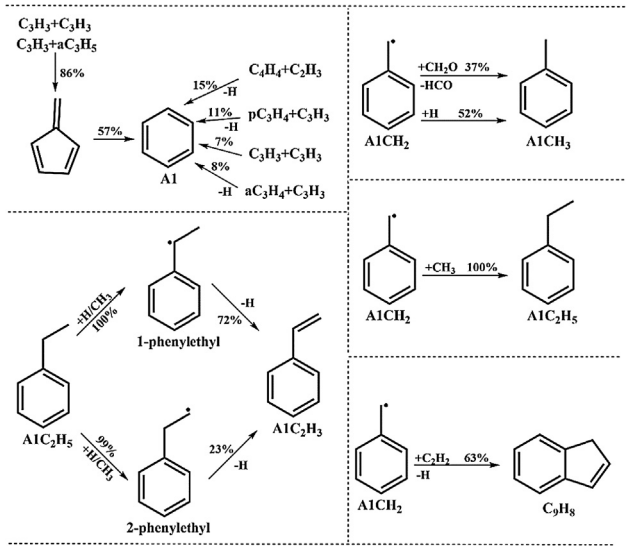

Fig. 10. Main formation network of aromatics in MD pyrolysis at 973 K, 760 Torr. Numbers beside arrows indicate the percentage of the carbon flux of corresponding pathway in total carbon flux of species formation.

generated from the reactions of $A1CH_2$ and CH_2O ($A1CH_2 + CH_2O = A1CH_3 + CHO$) and the H-addition reaction of $A1CH_2$ ($A1CH_2 + H = A1CH_3$) with a total 89% contribution. For the formation of styrene, its formation is entirely controlled by the β-C–H scission reaction of two C_8H_{11} radicals named 1-phenylethyl radical and 2-phenylethyl radical, which are the major products of ethylbenzene from H-abstraction reactions. For ethylbenzene, the second abundant aromatics detected in MD pyrolysis, it is chiefly produced by the combination reactions of $A1CH_2$ and CH_3 ($A1CH_2 + CH_3 = A1C_2H_5$). Furthermore, most indene is converted by the reaction of $A1CH_2$ and C_2H_2 ($A_1CH_2 + C_2H_2 = C_9H_8 + H$).

5. Conclusions

Flow reactor pyrolysis of MD was investigated from 773 to 1198 K at low and atmospheric pressures by using SVUV-PIMS. Various pyrolysates were detected, and their mole fraction profiles as functions of temperature were also evaluated. A kinetic model of MD pyrolysis with 286 species and 2165 reactions was constructed and used to validate the experimental data. On the basis of the modeling analysis, the decomposition of MD is totally controlled by the unimolecular dissociation and H-abstraction reactions at all investigated pressures. C_4-C_9 unsaturated esters are mainly derived from the β-C–C and β-C–H scission of methyl ester radicals, while the dominated formation channels of C_5-C_9 1-alkenes are the β-C–C scission of MD radicals. Furthermore, benzene and benzyl radical can be produced via combination reactions of small radicals and molecules, such as aC_3H_5, C_3H_3 C_2H_2 and C_5H_5, which are the products of 1-alkenes via unimolecular decomposition.

Acknowledgements

This research was supported by the National Key Scientific Instruments and Equipment Development Program of China (2012YQ22011305) and, the Natural Science Foundation of China (51676176 and 21373193).

Appendix A. Supplementary data

Supplementary data associated with this article can be found, in the online version, at http://dx.doi.org/10.1016/j.fuel.2018.05.145.

References

[1] Kohse-Hoinghaus K, Osswald P, Cool TA, Kasper T, Hansen N, Qi F. Biofuel combustion chemistry: from ethanol to biodiesel. Angew Chem Int Ed Engl 2010;49:3572–97.
[2] Aghbashlo M, Demirbas A. Biodiesel: hopes and dreads. Biofuel Res J 2016;3:379.
[3] Lin L, Ying D, Chaitep S, Vittayapadung S. Biodiesel production from crude rice bran oil and properties as fuel. Appl Energy 2009;86:681–8.
[4] Liu HY, Ma X, Li BW, Chen LF, Wang Z, Wang JX. Combustion and emission characteristics of a direct injection diesel engine fueled with biodiesel and PODE/biodiesel fuel blends. Fuel 2017;209:62–8.
[5] Demirbas A. Biodiesel production from vegetable oils via catalytic and non-catalytic supercritical methanol transesterification methods. Prog Energy Combust Sci 2005;31:466–87.
[6] Yang K, Wei L, Cheung CS, Tang CL, Huang ZH. The effect of pentanol addition on the particulate emission characteristics of a biodiesel operated diesel engine. Fuel 2017;209:132–40.
[7] Roy MM, Wang W, Bujold J. Biodiesel production and comparison of emissions of a DI diesel engine fueled by biodiesel–diesel and canola oil–diesel blends at high idling operations. Appl Energy 2013;106:198–208.
[8] Wei LJ, Cheng RP, Mao HJ, Geng P, Zhang YJ, You K. Combustion process and NOx emissions of a marine auxiliary diesel engine fuelled with waste cooking oil biodiesel blends. Energy 2018;144:73–80.
[9] Kumar N. Oxidative stability of biodiesel: causes, effects and prevention. Fuel 2017;190:328–50.
[10] Dooley S, Curran HJ, Simmie JM. Autoignition measurements and a validated kinetic model for the biodiesel surrogate, methyl butanoate. Combust Flame 2008;153:2–32.
[11] Zhou XY, Zhai YT, Ye LL, Zhang LD. Theoretical studies on the reaction kinetics of methyl crotonate with hydroxyl radical. Sustain Energy Fuels 2018;2:392–402.
[12] Fisher EM, Pitz WJ, Curran HJ, Westbrook CK. Detailed chemical kinetic mechanism for combustion of oxygenated fuels. Proc Combust Inst 2000;28:1579–86.
[13] Lin KC, Lai JYW, Violi A. The role of the methyl ester moiety in biodiesel combustion: a kinetic modeling comparison of methyl butanoate and n-butane. Fuel 2012;92:16–26.
[14] Diévart P, Won SH, Dooley S, Dryer FL, Ju Y. A kinetic model for methyl decanoate combustion. Combust Flame 2012;159:1793–805.
[15] Wang YL, Feng Q, Egolfopoulos FN, Tsotsis TT. Studies of C4 and C10 methyl ester flames. Combust Flame 2011;158:1507–19.
[16] Haylett DR, Davidson DF, Hanson RK. Ignition delay times of low-vapor-pressure fuels measured using an aerosol shock tube. Combust Flame 2012;159:552–61.
[17] Wang W, Oehlschlaeger MA. A shock tube study of methyl decanoate autoignition at elevated pressures. Combust Flame 2012;159:476–81.
[18] Li ZH, Wang WJ, Huang Z, Oehlschlaeger MA. Autoignition of methyl decanoate, a biodiesel surrogate, under high-pressure exhaust gas recirculation conditions. Energy Fuels 2012;26:4887–95.
[19] Sarathy SM, Thomson MJ, Pitz WJ, Lu T. An experimental and kinetic modeling study of methyl decanoate combustion. Proc Combust Inst 2011;33:399–405.
[20] Seshadri K, Lu T, Herbinet O, Humer S, Niemann U, Pitz WJ, et al. Experimental and kinetic modeling study of extinction and ignition of methyl decanoate in laminar non-premixed flows. Proc Combust Inst 2009;32:1067–74.

[21] Herbinet O, Pitz WJ, Westbrook CK. Detailed chemical kinetic oxidation mechanism for a biodiesel surrogate. Combust Flame 2008;154:507–28.
[22] Herbinet O, Pitz WJ, Westbrook CK. Detailed chemical kinetic mechanism for the oxidation of biodiesel fuels blend surrogate. Combust Flame 2010;157:893–908.
[23] Glaude PA, Herbinet O, Bax S, Biet J, Warth V, Battin-Leclerc F. Modeling of the oxidation of methyl esters-Validation for methyl hexanoate, methyl heptanoate, and methyl decanoate in a jet-stirred reactor. Combust Flame 2010;157:2035–50.
[24] Diévart P, Won SH, Gong J, Dooley S, Ju Y. A comparative study of the chemical kinetic characteristics of small methyl esters in diffusion flame extinction. Proc Combust Inst 2013;34:821–9.
[25] Grana R, Frassoldati A, Saggese C, Faravelli T, Ranzi E. A wide range kinetic modeling study of pyrolysis and oxidation of methyl butanoate and methyl decanoate – Note II: lumped kinetic model of decomposition and combustion of methyl esters up to methyl decanoate. Combust Flame 2012;159:2280–94.
[26] Luo ZL, Maciaszek T, Som MJ, Longman DE. A reduced mechanism for high-temperature oxidation of biodiesel surrogates. Energy Fuels. 2010;24:6283–93.
[27] Wang K, Villano SM, Dean AM. Impact of the molecular structure on olefin pyrolysis. Energy Fuels 2017;31:6515–24.
[28] Cai JH, Zhang LD, Zhang F, Wang ZD, Cheng ZJ, Yuan WH. Experimental and kinetic modeling study ofn-butanol pyrolysis and combustion. Energy Fuels. 2012;26:5550–68.
[29] Arad A, Sher E, Enden G. Modeling soot formation in diesel-biodiesel flames. Fuel 2017;206:437–52.
[30] Lund H. Renewable energy strategies for sustainable development. Energy 2007;32:912–9.
[31] Ullah K, Ahmad M, Sofia SharmaK, Lu P, Harvey A, et al. Assessing the potential of algal biomass opportunities for bioenergy industry: a review. Fuel 2015;143:414–23.
[32] Sharma VKF, Mincarini M, Berillo M, Cornacchia G. Disposal of waste tyres for energy recovery and safe environment. Appl Energy 2000;65:381–94.
[33] Czajczyńska D, Anguilano L, Ghazal H, Krzyżyńska R, Reynolds AJ, Spencer N, et al. Potential of pyrolysis processes in the waste management sector. Therm Sci Eng Prog 2017;3:171–97.
[34] Hrdlička J, Skopec P, Dlouhý T, Hrdlička F. Emission factors of gaseous pollutants from small scale combustion of biofuels. Fuel 2016;165:68–74.
[35] Herbinet O, Glaude PA, Warth V, Battin-Leclerc F. Experimental and modeling study of the thermal decomposition of methyl decanoate. Combust Flame 2011;158:1288–300.
[36] Pyl SP, Geem KMV, Puimège P, Sabbe MK, Reyniers MF, Marin GB. A comprehensive study of methyl decanoate pyrolysis. Energy 2012;43:146–60.
[37] Pines H, Haag WO. Alumina: catalyst and support. I. alumina, its intrinsic acidity and catalytic activity1. J Am Chem Soc 1960;82:2471–83.
[38] Maciver D, Tobin H, Barth R. Catalytic aluminas I. Surface chemistry of eta and gamma alumina. J Catal 1963;2:485–97.
[39] Wang ZD, Cheng ZJ, Yuan WH, Cai JH, Zhang LD, Zhang F. An experimental and kinetic modeling study of cyclohexane pyrolysis at low pressure. Combust Flame 2012;159:2243–53.
[40] Wang ZD, Bian HT, Wang YZ, Zhang LD, Li YY, Zhang F. Investigation on primary decomposition of ethylcyclohexane at atmospheric pressure. Proc Combust Inst 2015;35:367–75.
[41] Cheng ZJ, Tan YY, Wei LX, Xing LL, Yang JZ, Zhang LD. Experimental and kinetic modeling studies of furan pyrolysis: fuel decomposition and aromatic ring formation. Fuel 2017;206:239–47.
[42] Sun WY, Tao T, Zhang R, Li W, Yang JZ, Yang B. Elucidating the flame chemistry of monoglyme via experimental and modeling approaches. Combust Flame 2018;191:298–308.
[43] Zeng MR, Yuan WH, Wang YZ, Zhou WX, Zhang LD, Qi F. Experimental and kinetic modeling study of pyrolysis and oxidation of n-decane. Combust Flame 2014;161:1701–15.
[44] Wang ZD, Zhao L, Wang YZ, Bian HT, Zhang LD, Zhang F. Kinetics of ethylcyclohexane pyrolysis and oxidation: an experimental and detailed kinetic modeling study. Combust Flame 2015;162:2873–92.
[45] Farooq A, Ren W, Lam KY, Davidson DF, Hanson RK, Westbrook CK. Shock tube studies of methyl butanoate pyrolysis with relevance to biodiesel. Combust Flame 2012;159:3235–41.
[46] Luo YR. Comprehensive handbook of chemical bond energies CRC Press; 2007.
[47] Ning HB, Wu JJ, Ma L, Ren W, Davidson DF, Hanson RK. Chemical kinetic modeling and shock tube study of methyl propanoate decomposition. Combust Flame 2017;184:30–40.
[48] Rodriguez A, Herbinet O, Battin-Leclerc F, Frassoldati A, Faravelli T, Ranzi E. Experimental and modeling investigation of the effect of the unsaturation degree on the gas-phase oxidation of fatty acid methyl esters found in biodiesel fuels. Combust Flame 2016;164:346–62.
[49] Zhao L, Xie MF, Ye LL, Cheng ZJ, Cai JH, Li YY. An experimental and modeling study of methyl propanoate pyrolysis at low pressure. Combust Flame 2013;160:1958–66.
[50] Sun WY, Yang B, Hansen N, Westbrook CK, Zhang F, Wang G. An experimental and kinetic modeling study on dimethyl carbonate (DMC) pyrolysis and combustion. Combust Flame 2016;164:224–38.
[51] Yuan WH, Li YY, Dagaut P, Yang JZ, Qi F. Investigation on the pyrolysis and oxidation of toluene over a wide range conditions. I. Flow reactor pyrolysis and jet stirred reactor oxidation. Combust Flame 2015;162:3–21.
[52] Chemkin-Pro 15092, Reaction Design, San Diego; 2009.
[53] Wang H, Sheen DA. Combustion kinetic model uncertainty quantification, propagation and minimization. Prog Energy Combust Sci 2015;47:1–31.
[54] Dickinson RP, Gelinas RJ. Sensitivity analysis of ordinary differential equation systems—A direct method. J Comput Phys 1976;21:123–43.
[55] Turányi T. Applications of sensitivity analysis to combustion chemistry. Reliab Eng Syst Safe 1997;57:41–8.
[56] Oyeyemi VB, Dieterich JM, Krisiloff DB, Tan T, Carter EA. Bond dissociation energies of C_{10} and C_{18} methyl esters from local multireference averaged-coupled pair functional theory. J Phys Chem A 2015;119:3429–39.
[57] Zhai YT, Feng BB, Yuan WH, Ao CC, Zhang LD. Experimental and modeling studies of small typical methyl esters pyrolysis: methyl butanoate and methyl crotonate. Combust Flame 2018;191:160–74.
[58] Zhang LD, Zhang P. Towards high-level theoretical studies of large biodiesel molecules: an ONIOM [QCISD(T)/CBS:DFT] study of hydrogen abstraction reactions of $C_{(n)}H_{(2n+1)}COOC_{(m)}H_{(2m+1)}$ + H. Phys Chem Chem Phys 2015;17:200–8.
[59] Oyeyemi VB, Keith JA, Carter EA. Accurate bond energies of biodiesel methyl esters from multireference averaged coupled-pair functional calculations. J Phys Chem A 2014;118:7392–403.
[60] Fan XY, Wang G, Li YY, Wang ZD, Yuan WH, Zhao L. Experimental and kinetic modeling study of 1-hexene combustion at various pressures. Combust Flame 2016;173:151–60.